University College London
Rutherford Appleton Laboratory

Activity Report

for the first year of the course of Ph.D. in Particle Physics

L. Cerrito

July 1999

Contents

1 Introduction

This report is an overview of my activity in the past few months in the CDF (Collider Detector at Fermilab) experiment. The CDF is a general purpose experiment for the study of $p\bar{p}$ collisions at $\sqrt{s} = 1.8\ TeV$ at the Fermilab Tevatron Collider. After over 10 years of activity and a performance evolution, of the Tevatron and CDF together, to yield data sets of ever increasing sensitivity in Run 0 and Run I, the Tevatron Collider remains for the Run II the highest energy machine. The stated goal of Tevatron Run II is the accumulation of 2 fb^{-1} at $\sqrt{s} = 2.0\ TeV$, using luminosities up to $2 \times 10^{32}\ cm^{-2}s^{-1}$.

Precision capability at the energy frontier will allow attack on the open questions of high energy physics, including direct search for new phenomena, a global precision electroweak program, constraint of the CKM matrix with high statistic B decays, test of perturbative QCD at Next-to-Leading-Order and large Q^2.

The high luminosity Tevatron of Run II requires extensive changes to the experimental apparatus for CDF [1]. In particular the tracking system will be replaced with a new and more optimal combination of drift chamber and silicon vertex detector. The calorimetry will be exclusively scintillator based, the electronics and trigger will be fully compliant with the new pipelined configuration, and all the software is being re-written using C++ and an Object Oriented architecture. The CDF Run II is due to start in April 2000 and a first run with cosmic rays will be done in September 1999.

My activity has developed in two directions, on one side working for the Run II upgrade, and in particular within the commitments of the University College London group, that will be responsible for the alignment and calibration procedure of the central drift chamber (COT). Secondly I have been focusing my interests on an area of work for a data analysis using Run I data. Therefore this report is divided in two sections, the first describes briefly the fitting procedure and shows the impact of the alignment correction on fitted muon tracks, whereas the second part describes the physics topic that I am currently pursuing with a view to completing a thesis topic based on a sample of B events from the Run I CDF data.

2 TrackFit in the Central Outer Tracker for the Run II at CDF

Efficient, precision charged particle tracking is a crucial aspect for the CDF physics analysis. Among the applications of charged particle tracking are, for example, the reconstruction of track momentum for measurements at both high (M_W) and low ($B \to J/\psi K$) p_T, or precision reconstruction of track impact parameter for B physics. The tracking system uses a central drift chamber and a silicon "inner tracker", built from a micro-vertex detector and two additional silicon layers at intermediate radii.

The Central Outer Tracker (COT) [2] is an open cell drift chamber designed to replace, in the region $\mid \eta \mid \leq 1.0$, the Central Tracking Chamber (CTC) used in Run 0 and Run I, which would suffer from severe occupancy problems at luminosities $\mathcal{L} \geq 1 \times 10^{32}\ cm^{-2}s^{-1}$. The design goal of the COT is to reproduce the functionality of the CTC, but using smaller drift cells and a fast gas to limit drift times to less than 100 ns. The cells in the COT are grouped in 8 super-layers, covering a radial span between 44 cm and 132 cm. A deficiency in CTC stereo reconstruction, caused by the small number of stereo measurements (24 out of the 84 total), will be removed by increasing the number of stereo measurements to 48 out of the 96 total measurements.

Since the COT is designed to operate with a maximum drift of 100 ns (compared with 706 ns for the CTC) a drift velocity of $\sim$ 100 $\mu m/ns$ implies a maximum drift distance of $\sim$ 1 cm, about 1/4 that of the CTC. The COT will then have about 4 times the number of cells, with a total of 2,520 drift cells and 30,240 readout channels for the entire detector. The smaller drift length allows a smaller cell tilt. For an electric field of $\sim$ 2.5 kV/cm (compared with 1.3 kV/cm in the CTC) the Lorentz angle for the COT is 35° (compared with 45° in the CTC).

The basic drift cell has a line of 12 sense wires alternating with shaper wires every 3.8 mm, running down the middle of two gold-on-mylar cathode planes which are separated by $\sim$ 2 cm. The wires and cathode planes are strung between two precision milled end-plates, and the complete chamber is roughly 1.3% of a radiation length at normal incidence. Stereo cells will be strung using an offset between slots on opposing end-plates. With an eight cell offset the COT has the same nominal 3° stereo angle as the CTC.

The similarity of the COT and CTC geometries allows Tracking and Fitting procedures to be used by switching to the appropriate geometric configuration of the chamber. The following description will be valid for both the detectors and the code for tracking and fitting is intended to work for the COT as well as for the old CTC. The ability to debug COT tracking algorithms using real Run I data has proved to be very valuable and in debugging and in understanding the COT operation, where at the present only MC data is available.

2.1 The Fitting procedure

The fitting procedure is the process which takes a set of hits in the detector, identified as belonging to a track by the pattern recognition code, and fits them to a helix, using all the available information coming from the central tracking chamber. The trajectory of a charged particle in a uniform magnetic field $\vec{B}$ is a helix, for which the projection onto the $r - \phi$ plane (perpendicular to $\vec{B}$) is a circle with radius:

$$R = p_T/qB \tag{1}$$

where q is the electric charge and p_T the momentum of the particle in the $r-\phi$ plane. This helix is parametrized by five numbers: curvature c (inverse radius of the circle in $r-\phi$); impact parameter d_0 (distance of closest approach to $r=0$); ϕ_0 (azimuthal direction at the point of closest approach to $r=0$); z_0 (the z position at the point of closest approach to $r=0$); and $cot\theta$, where θ is the polar angle.

There is a list of effects that have to be taken into account by the trackfit. Non uniformities in magnetic and electric field, misalignment of the tracking chamber, changing in drift velocity with the distance from the wire or dependence with the aspect angle of the track. All these factors have potentially sensitive consequences on the physics. At the trackfit level these effects have to be corrected to avoid systematic errors in reconstructing the charged particle trajectories.

The fit in CTC and COT is done using a χ^2 minimization technique [3], searching for the point:

$$\vec{\nabla}_{\vec{p}}\chi^2 = 0 \tag{2}$$

where $\vec{p}$ are the set of fit parameters. A simple χ^2 which can be used in the minimization algorithm is the following:

$$\chi^2 = \sum_{hits} \frac{(\tilde{D}_h(\vec{p}) - D_h)^2}{\sigma_h^2} \tag{3}$$

where $\tilde{D}(\vec{p})$ is the predicted drift distance for hit h, D_h is the measured drift distance, and σ_h is the resolution of D_h. The predicted drift distance is evaluated by using the drift direction, the sense wire positions and the parameters of the track. This gives a quadratic equation in the drift distance.

The measured drift distance is obtained combining the measured drift time, the drift properties and the wire positions. The equation is of the form:

$$\begin{aligned} D &= (t - t_0)v \\ \vec{r} &= \vec{r}_w + D\hat{v} \end{aligned} \tag{4}$$

where $\vec{v}$ is constant (per layer), but t_0 is assumed to be only approximately constant. All short-comings of this linear drift model are lumped into t_0, which is allowed to vary with both the measured properties of the hit (the turn-on time and the time-over-threshold) and - when this information is available - with the track parameters.

The determination of predicted and measured displacement, $\tilde{D}_h(\vec{p})$ and D_h, is the stage where most of the corrections, due to the deviation from the nominal geometry and behaviour of the tracking chamber, are taken into account. Among them, wire sag and per-layer alignment terms, which I will describe in more details in the next section. Several effects which enter in the determination of the measured displacement, and in particular in t_0, are the following:

Corrections which do not require knowing the track parameters:

- Channel dependence. The delay in going through the analog pulse shaping and discriminator varies from channel to channel.
- Run dependence. There are variations in t_0.
- Leading-edge (t) dependence. The drift velocity rises slightly very near the sense wire. This is corrected by having t_0 vary linearly with t for $t < t_{max}/4$.
- Time-slewing correction. The point on the leading edge at which the discriminator fires varies with the amplitude of the pulse. The width, i.e. time over threshold, of the pulse also varies with the amplitude. t_0 is adjusted with the pulse width to correct for this.

Corrections which require an estimate of the track parameters:

- Time-of-flight and signal propagation time corrections.
- "Aspect angle" dependence. The drift trajectory (direction, not magnitude) is non-linear near the sense wire. This is corrected by having t_0 vary with the $r - \phi$ angle between the track and the nominal drift direction.
- Interaction time dependence. The spread of the beam gives an approximate 2 ns spread in interaction time. The interaction time is estimated on the base of the hit residuals of all tracks associated with a vertex, then re-fit the tracks correcting for this.
- "Miscellaneous" corrections, i.e. a tabular correction versus aspect angle and leading-edge time with no attempt to understand what the corrections are due to.

All these corrections were implemented in the CTC Tracking code, either at fitting level or, when track parameters are not required, at earlier stage. The specific task currently is to make available a new tracking code, written in C++ and inserted within the Run II software framework, which can work for both CTC and COT chambers and reproduce the functionality of the old code as well as, where possible, to improve its performance. At the moment two possible strategies are being pursued: one is developing a new code that mirrors strictly the old Fortran version, the other is developing a completely new code and adding, step by step, the necessary corrections.

2.2 Alignment corrections

In this section I will describe the alignment corrections that I have implemented to the Trackfit code and show their impact on the fitted helix parameters. The CTC/COT measures for each track an angle ϕ_i at each layer. A systematic error in ϕ_i can clearly bias the fitted helix parameters. For instance, an error of the form $\phi_i \rightarrow \phi_i + kr_i$ generates a "false curvature" $c \rightarrow c + 2k$, while an error of the form $\phi_i + \epsilon s_i z(r_i)$, i.e. with a z dependence, modifies $\lambda = cot\theta$ by $\lambda \rightarrow \lambda(1 + 2\epsilon < r >)$ without scaling z_0.

The internal alignment [4] is intended to remove systematic errors of the form $\phi_i \rightarrow \phi_i + A_i + B_i z(r_i)$. The physical model for these misalignments is a coherent (i.e. ϕ independent) twist of each end-plate as a function of radius. To allow different deformations in the east and west end-plates, the ϕ offsets are given a linear slope in z. The Run Ib alignment offsets for run 57279 at $z = \pm 150\ cm$ are shown in figure 1. Displacements, for layers, that vary too rapidly as can

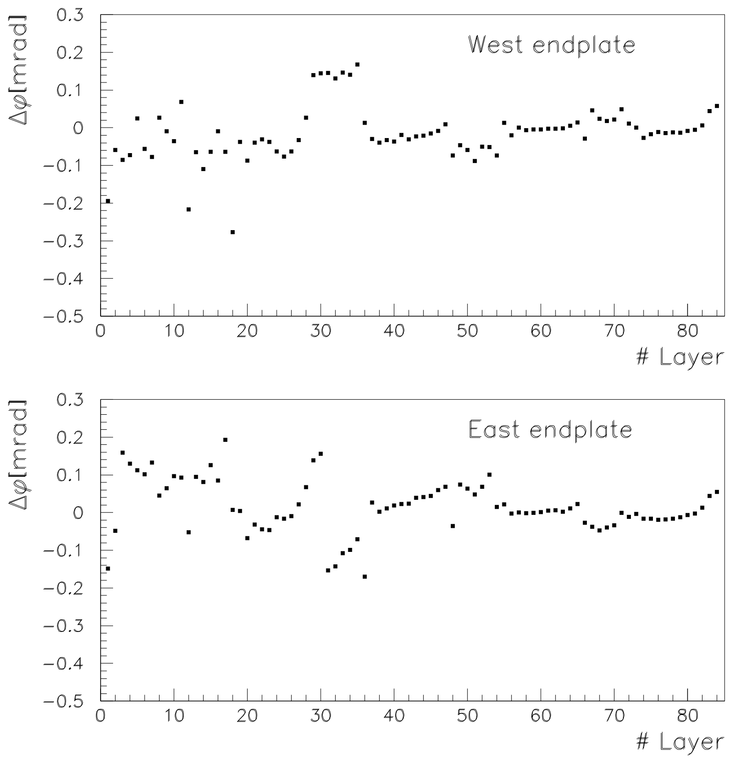

Figure 1: Run I ϕ offsets vs. CTC layer number at end-plates. The $\Delta\phi$ values are calculated from the WPO constants for run 57279.

be seen at inner and outer layers of some super-layers, are believed to be caused by the small correlation between alignment and calibration, i.e some drift model effects can be absorbed by the alignment constants. A false curvature can be seen here as a difference of about 0.2 $mrad$ from inside to outside in the east end-plate alignment. A much smaller effect can be seen in the west end-plate. In the old CTC tracking code the correction for the wire position offsets (WPO) is included by adjusting the drift distance. In the new tracking code, I implemented a rotation of the nominal wire position at end-plates as described by the WPO constants. Each wire of a basic cell is described in a frame where the y coordinate of the center of the cell is zero and the cell is tilted with respect to the y axis by the Lorentz angle, as shown in fig. 2. All the wires in the tracking chamber are reached by rotating the basic cell of the appropriate angle. Wire Position Offsets are included by adding a $\Delta\phi$ to this rotation. A slope, which is induced on axial layers, or modified from the nominal on stereo layers, is entered as $\Delta\phi(z_{max})$ at east and west end-plates.

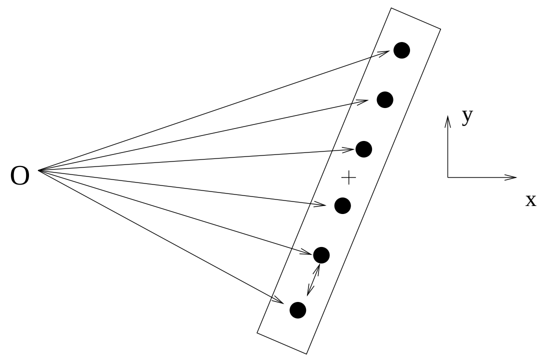

Figure 2: Geometric representation of a basic six-wires cell in CTC. All the wires in the tracking chamber are reached by rotating the vectors by 2π(number of the cell/total number of cells for that layer)

The sag of the wires is taken into account by allowing for a quadratic term into the equation that describes the wire. A wire is described by:

$$\begin{pmatrix} x \\ y \end{pmatrix}(z) = \begin{pmatrix} x_0 \\ y_0 \end{pmatrix} + \begin{pmatrix} a_x \\ a_y \end{pmatrix} z^2 + \begin{pmatrix} b_x \\ b_y \end{pmatrix} z \tag{5}$$

A wire sag has presently only been implemented in the y direction, due to the gravitation, with no component along x. In the $z - y$ plane, the coefficients are determined by the sense wire sag s (230 μm for CTC) from the end-plates to $z = 0$. The equation for the y component becomes now:

$$y = (y_0 - s) + \left(\frac{s}{z_{end}^2}\right) z^2 + b_y z \tag{6}$$

where b is determined by the stereo angle and the WPO relative rotation at the end-plates.

After having implemented alignment and sag corrections in the fitting code the set of hits belonging to muon tracks, from $Z \to \mu\mu$ Run I events, has been

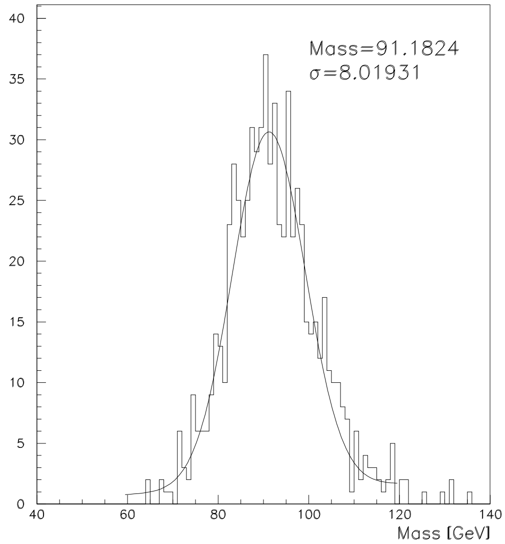

Figure 3: Z mass from $\mu\mu$ tracks re-fitted after having implemented alignment corrections.

re-fitted. In figure 3 the Z mass peak coming from $Z \rightarrow \mu\mu$ is shown. The number of events is 718. The curve is a Gaussian fit with a linear background and the peak is at $M = 91.18\ GeV$ with a σ of $8.0\ GeV$.

Figure 4 shows the effect of the alignment corrections on $1/p_T$ (p_T is the transverse momentum of the track calculated from the curvature of the helix). Plotted is the difference $\Delta(1/p_T)[\%]$ between the tracks fitted with and without alignment correction. The plot is made separately for positive and negative charged muons. Positive tracks are shifted by $+0.22 \pm 0.05$ %, whereas negative tracks are shifted by -0.27 ± 0.05 %. The wire position offset is therefore responsible for generating a "false curvature" of about 0.2% which is very significant since, for instance, the statistical precision of determining the momentum scale from $Z \rightarrow \mu\mu$ events is $\sim$ 0.1% and this is a direct input into the W mass determination.

Taking into account rotations of the end-plates, misalignments and wire sag is then important as the result can affect, at a sensitive level, the estimate of the track parameters. The next step will be to include calibration corrections, e.g. correcting for non-linearities in drift model. At the end we intend to reach the same performance, or hopefully better, as the old Fortran-based fitter. This will also provide a good introduction for understanding the alignment and calibration of the COT when CDF Run II will start collecting data.

t

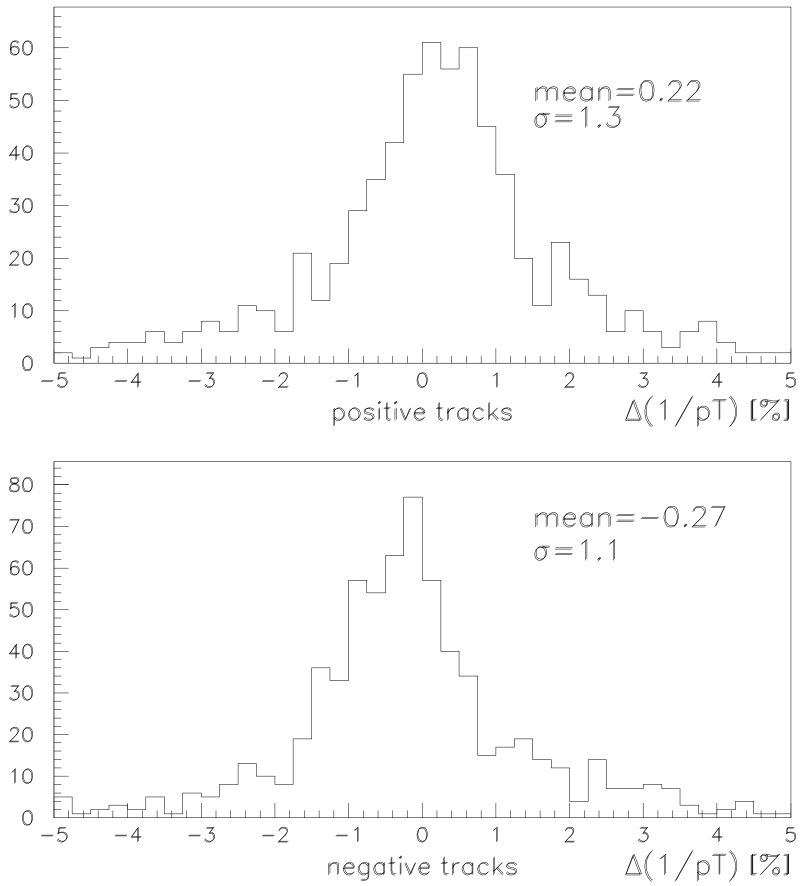

Figure 4: Impact of the alignment corrections on positive and negative muon tracks (upper and lower plot). The difference of $1/p_T$ has been taken between tracks fitted with and without alignment corrections. Notice that the shift has opposite sign for positive and negative tracks.

3 Scalar Couplings in Semileptonic B Decay

CDF has published many papers on b-properties, e.g. masses, lifetimes, and has made the first measurement indicating CP violation in the b-system. The b-sector is also a promising area in which to search for evidence of physics beyond the Standard Model (SM). There are many theoretical reasons for extending the Standard Model and a general feature of these extensions is that more Higgs particles are present and they have a much richer phenomenology than that of the Higgs particle in the SM [5].

Higgs particles are a crucial ingredient of gauge theories of the electro-weak interaction. In these theories some of the scalar particles become the longitudinal part of massive gauge bosons by the Higgs mechanism, while the other scalar particles, called Higgs particles, will manifest themselves as real. In the Standard Model a single neutral Higgs is left over after symmetry breaking. To break a SU(2) gauge symmetry the simplest possibility is to introduce a doublet of complex scalar fields H. Under spontaneous breaking of such symmetry, three of the four degrees of freedom of H will give mass to the three bosons of the theory, whereas the forth gives rise to a massive scalar particle.

The experimental search for the Higgs in the Standard Model is very difficult since it is electrically neutral, conserves flavor and parity, and it couples very weakly to low-mass fermions. However, if the Standard Model is not the complete theory of the electroweak interaction, there should exist additional Higgs particles which do not have to conserve flavor, might have electric charge, etc. Charged Higgs can, for example, mediate $B \to D\ \mu\ \nu$ processes [8][9], but the scalar nature of the Higgs will now determine a scalar dynamic. By identifying the scalar coupling as a charged Higgs mediating the decay, one may extract the relative $H^{\pm}/W^{\pm}$ coupling strengths.

For the general semileptonic meson decay:

$$M \to m\ l\ \nu,$$

where M and m are two pseudoscalar mesons and l and ν refer to the charged lepton and its neutrino, the most general Lorentz invariant form of the matrix element of this decay is [6]:

$$M = \frac{G_F}{\sqrt{2}} V_{ij} \bar{u}(p_\nu)(1+\gamma^5)\left\{ M f_S - \frac{1}{2}\left[(P+p)_\alpha f_+ + (P-p)_\alpha f_-\right]\gamma^\alpha + i\frac{f_T}{M}\sigma_{\alpha\beta}P^\alpha p^\beta \right\} v(p_l) \tag{7}$$

where G_F is the Fermi coupling constant, V_{ij} is the appropriate Cabibbo-Kobayashi-Maskawa (CKM) matrix element and P, p and M, m are the 4-momenta and masses of the M and m mesons respectively. Equation (7) consists of a scalar, a vector and a tensor terms, where the form factors f_S, $f_\pm$ and f_T are functions of the squared momentum transfer to leptons $Q^2 = (P-p)^2$. Two of the form factors, f_+ and f_-, arise from a vector particle mediating the decay while the remaining form factors, f_S and f_T, come from scalar and tensor exchange. This transition amplitude provide then a measure of the admixture of different dynamics or coupling occurring in the decay.

The decay rate can be calculated in the rest frame of the parent meson and it is:

$$\Gamma(E_m, E_l) \propto A \cdot |V|^2 + B \cdot \Re(V^* S) + C \cdot |S|^2 \tag{8}$$

where A, B and C are combinations of the kinematic variables of the decay and S, V are the effective vector and scalar terms [7]:

$$\begin{array}{l} V = f_+ + \frac{m_l}{M} f_T \\ S = f_S + (\frac{m_l}{2M} f_-) + \frac{(P+p)_\alpha (p_\nu - p_l)^\alpha}{2M^2} f_T \end{array} \tag{9}$$

or also

$$S = f_S + \frac{m_l}{2M} f_- + \left\{ \frac{(E_\nu - E_l)}{M} + \frac{m_l^2}{2M^2} \right\} f_T$$

obtained collapsing the terms in equation (7), involving f_- and f_T, into induced vector and scalar components.

The equation (9) shows that the induced scalar coupling is suppressed for heavy mesons decaying into light leptons by the factor m_l/M, whereas eq. (8) express how the decay rate is affected by couplings non predicted by the SM. The appearance of a considerable nonzero scalar and tensor form factors points to deviations from the standard V-A interaction [10].

The shape of the Dailitz plot for semileptonic decays, and in particular for $B^0 \to D^- \mu^+ \nu$, is extremely sensitive to the appearance of scalar contributions into the Lorentz structure of the coupling [11][12]. In figure 5 is plotted the phase space density contours for decays of $B^0 \to D^- \mu^+ \nu$ showing the effects of scalar, vector and tensor couplings in the decay. The figure has been taken from [6].

The advantages of using B's in muonic decays are in a larger coupling of the Higgs with the muon, and reduced electromagnetic radiative effects, although the suppression of the induced scalar term (f_-) for muonic decays is less than for electronic decays.

The presence of a neutrino in the final state means ambiguities can arise in the reconstruction of the final state kinematics and this will limit the sensitivity with which it is possible to isolate non-standard contributions to the Dailitz plot. I am just beginning MC studies to evaluate the limits it would be possible to place on charged Higgs production using this method.

4 Summary

An outline of my activity at CDF have been given in the two sections of this report. I have described the alignment corrections to the trackfit in the central drift chamber, within the context of the more general fitting procedure, and

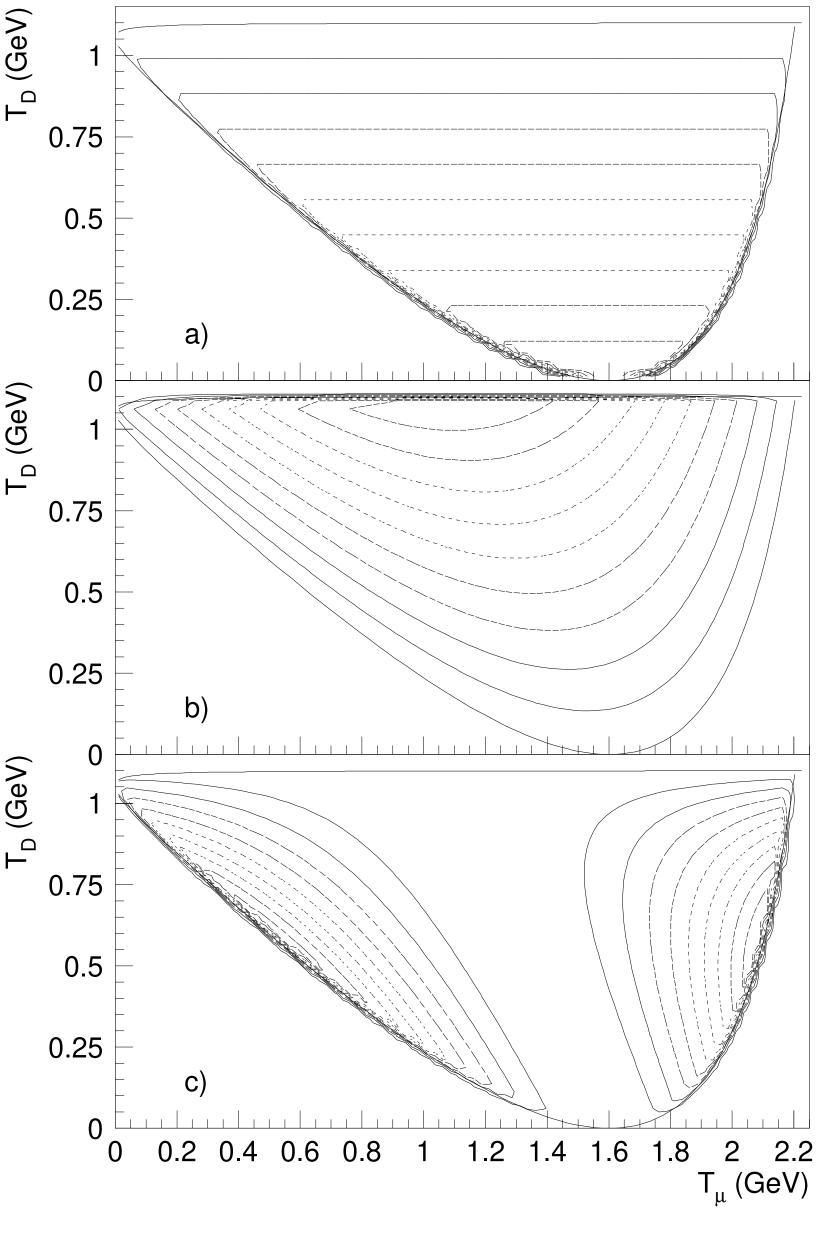

Figure 5: Phase space density contours for decays of $B^0 \rightarrow D^- \mu^+ \nu$ showing effects of a) scalar, b) vector and c) tensor couplings in the decay. These figures have been taken from [6]. The variables plotted are the D^- and μ^+ kinetic energies (T_D, T_μ). The dark contour shows where the phase space density is higher.

showed the importance of these corrections for the evaluation of the curvature of the tracks. The next step will be to implement the required calibration corrections for an optimal trackfit in the COT.

In the last section I have described the physics topic that I am currently pursuing with a view to completing a thesis topic based on a sample of B events from the Run I CDF data.

References

[1] CDF collaboration, *Technical Design Report*, 1996.

[2] B. Ashmanskas *et* al., CDF note 3648 (1996).

[3] A. Mukherjee, CTC and VTX Tracking, CDF note, 1995.

[4] B. Ashmanskas, CDF note 4456 (1998).

[5] B. McWilliams and Ling-Fong-li, *Nucl. Phys.* B179 (1981) 62-84.

[6] R.J. Tesarek, eprint hep-ph/9901325 v2, (1999).

[7] M.V. Chizhov, eprint hep-ph/9511287 (1995).

[8] A. Falk, eprint hep-ph/9812217, (1998).

[9] A. Le Yaouanc *et* al., eprint hep-ph/9403341 (1994).

[10] A.A. Poblaguev, *Phys. Lett.* B 238 (1990) 108-111.

[11] J.D. Richman, eprint Stanford-HEP 95-01 (1995).

[12] M. Neubert, *Phys. Rep.* 245 (1994) 259-395.